Role of His505 in the Soluble Fumarate Reductase from *Shewanella frigidimarina*†

Katherine L. Pankhurst,‡ Christopher G. Mowat,‡,§ Caroline S. Miles,§ David Leys,# Malcolm D. Walkinshaw,§ Graeme A. Reid,§ and Stephen K. Chapman*,‡

Department of Chemistry, University of Edinburgh, West Mains Road, Edinburgh EH9 3JJ, United Kingdom, Institute of Cell and Molecular Biology, University of Edinburgh, Mayfield Road, Edinburgh EH9 3JR, United Kingdom, and Department of Biochemistry, Adrian Building, University of Leicester, University Road, Leicester LE1 7RH, United Kingdom

Received February 21, 2002; Revised Manuscript Received April 4, 2002

ABSTRACT: The X-ray structure of the soluble fumarate reductase from *Shewanella frigidimarina* [Taylor, P., Pealing, S. L., Reid, G. A., Chapman, S. K., and Walkinshaw, M. D. (1999) *Nat. Struct. Biol. 6*, 1108−1112] clearly shows the presence of an internally bound sodium ion. This sodium ion is coordinated by one solvent water molecule (Wat912) and five backbone carbonyl oxygens from Thr506, Met507, Gly508, Glu534, and Thr536 in what is best described as octahedral geometry (despite the rather long distance from the sodium ion to the backbone oxygen of Met507 (3.1 Å)). The water ligand (Wat912) is, in turn, hydrogen bonded to the imidazole ring of His505. This histidine residue is adjacent to His504, a key active-site residue thought to be responsible for the observed pK_a of the enzyme. Thus, it is possible that His505 may be important in both maintaining the sodium site and in influencing the active site. Here we describe the crystallographic and kinetic characterization of the H505A and H505Y mutant forms of the *Shewanella* fumarate reductase. The crystal structures of both mutant forms of the enzyme have been solved to 1.8 and 2.0 Å resolution, respectively. Both show the presence of the sodium ion in the equivalent position to that found in the wild-type enzyme. The structure of the H505A mutant shows the presence of two water molecules in place of the His505 side-chain which form part of a hydrogen-bonding network with Wat48, a ligand to the sodium ion. The structure of the H505Y mutant shows the hydroxyl group of the tyrosine side-chain hydrogen-bonding to a water molecule which is also a ligand to the sodium ion. Apart from these features, there are no significant structural alterations as a result of either substitution. Both the mutant enzymes are catalytically active but show markedly different pH profiles compared to the wild-type enzyme. At high pH (above 8.5), the wild type and mutant enzymes have very similar activities. However, at low pH (6.0), the H505A mutant enzyme is some 20-fold less active than wild-type. The combined crystallographic and kinetic results suggest that His505 is not essential for sodium binding but does affect catalytic activity perhaps by influencing the pK_a of the adjacent His504.

In the absence of oxygen, many bacteria are able to use fumarate as a terminal electron acceptor for respiration. In the majority of organisms, these fumarate reductases (which are closely related to succinate dehydrogenase) are bound to the inner face of the cytoplasmic membrane and contain both iron−sulfur centers and FAD[1] (*1*, *2*). However, in *Shewanella* species a soluble, periplasmic fumarate reductase is produced. The presence of four *c*-type heme groups and one FAD has led to this enzyme being designated as flavocytochrome c_3 (Fcc_3) (*3*). Examination of the crystal structures of the fumarate reductases from *Escherichia coli* (PDB entry 1FUM (1)), *Wolinella succinogenes* (1QLA, 1QLB (*4*), 1E7P (*5*)) and *Shewanella* species (1QJD (*6*), 1D4E (*7*), 1QO8 (*8*)) shows a clear conservation of the active site architecture. This is consistent with a universal mechanism for fumarate reduction in all the enzymes (*6*, *9*−*11*).

The highest resolution (1.8 Å) fumarate reductase structure is that for Fcc_3 from *Shewanella frigidimarina* (1QJD) (*6*). Close examination of this structure reveals the presence of an internally bound sodium ion (*6*, *12*). This sodium ion is tightly held and is clearly seen in electrospray mass spectrometry of wild-type and mutant forms of Fcc_3 (*9*, *11*). In the Fcc_3 structure (1QJD), the sodium ion is coordinated by five backbone carbonyl oxygen atoms (from T506, M507, G508, E534, and T536) and one solvent water molecule (Wat912) (Figure 1) in a geometry close to octahedral. These observations, together with the fact that the sodium ion lies close to both the FAD and the active site, led to the

† This work was supported by the UK Biotechnology and Biological Sciences Research Council (BBSRC) and by the Wellcome Trust funded Edinburgh Protein Interaction Centre (EPIC). K.P. acknowledges studentship funding from the EPSRC. We thank SRS Daresbury (station 9.6) for the use of synchrotron facilities. Synchrotron access at EMBL Hamburg was supported by the European Community - Access to Research Infrastructure Action of the Improving Human Potential Programme to the EMBL Hamburg Outstation, contract number HPRI-CT-1999-00017.

* To whom correspondence should be addressed. Prof. S. K. Chapman, Department of Chemistry, University of Edinburgh,West Mains Road, Edinburgh EH9 3JJ, U.K. E-mail: S.K.Chapman@ed.ac.uk. Fax/phone (44) 131 650 4760.

‡ Department of Chemistry, University of Edinburgh.

§ Institute of Cell and Molecular Biology, University of Edinburgh.

University of Leicester.

[1] Abbreviations: Fcc_3, flavocytochrome c_3; H505A, histidine505 → alanine mutation; H505Y, histidine505 → tyrosine mutation; FAD, flavin adenine dinucleotide

10.1021/bi020155e CCC: $22.00
Published on Web 06/18/2002

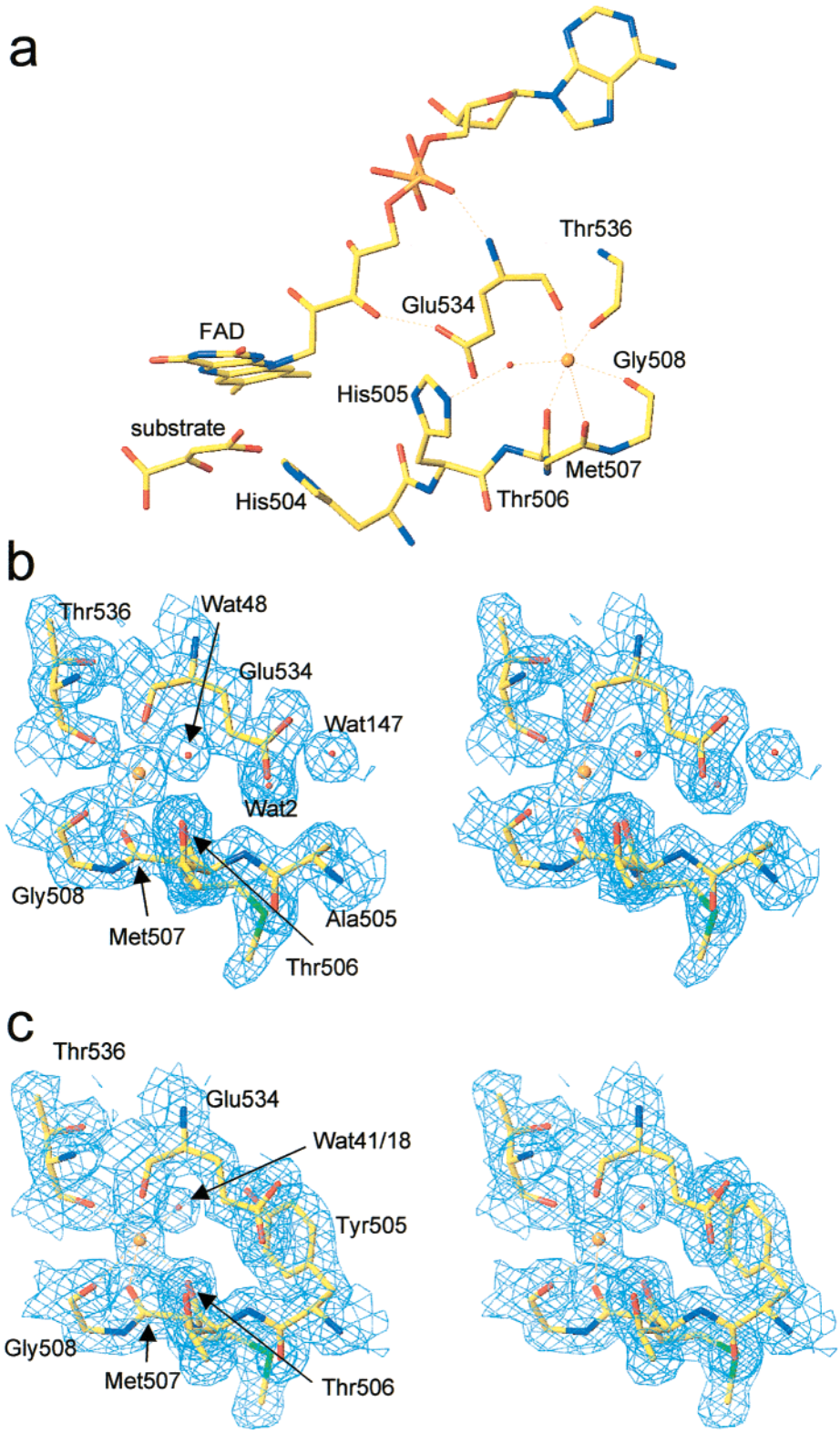

FIGURE 1: Panel (a) shows the region surrounding the internal bound sodium ion in flavocytochrome c_3. The sodium is shown in orange. Interactions with ligating oxygen atoms are shown as dotted lines, as are some hydrogen-bonding interactions. All sodium to ligand distances are 2.4 Å, except for that involving Met507, which is 3.1 Å. Panels (b) and (c) show the electron density surrounding the region of the internal bound sodium ion in the crystal structures of the H505A and H505Y mutant forms of flavocytochrome c_3, respectively. The sodium ion is shown in orange. Interactions between the sodium and the ligating oxygen atoms are shown as orange dotted lines. Electron density maps were calculated using Fourier coefficients $2F_o - F_c$. Where F_o and F_c are the observed and calculated structure factors, respectively, the latter based on the final model. The contour level is 1σ, where σ is the rms electron density. The figure was generated using TURBO−FRODO (*21*).

suggestion that it might play an important structural or regulatory role in the enzyme (*12*). An interesting feature of the sodium ion site is that the water ligand (Wat912) is hydrogen-bonded to His505, which is, in turn, next to a key substrate-binding residue, His504. In the present paper, we report an investigation into the importance of His505 in terms

of maintaining the integrity of the sodium site and affecting catalysis. We describe the kinetic characterization of the H505A and H505Y mutant enzymes together with their high-resolution X-ray crystal structures.

MATERIALS AND METHODS

DNA Manipulation, Strains, Media, and Growth. The mutant enzymes H505A-Fcc_3 and H505Y-Fcc_3 were generated by site-directed mutagenesis using the method of Kunkel and Roberts (*13*) as described previously (*3*, *9*).

Mutagenic oligonucleotides CCTGGTGTTCACGCTACTATGGGTGGC (which substitutes histidine 505 with alanine) and GGTGTTCACTACACTATGGG (which substitutes histidine 505 with tyrosine) were used. Mismatched bases are underlined. Screening for the H505A and H505Y mutations was carried out by sequencing of single stranded DNA. Dideoxy chain termination sequencing (*14*) using the Sequenase version 2.0 kit (United States Biochemicals) was carried out for the former and automated sequencing on a Perkin-Elmer ABI Prism 377 instrument for the latter. Both mutated *fccA* coding sequences were fully sequenced from single stranded DNA to check that no secondary mutations had been introduced.

The modified coding sequences were cloned into the broad-host range expression plasmid pMMB503EH (*15*) on an ~1.8 kbp *Eco*RI−*Hin*dIII fragment to generate pCM89 (H505A *fccA*/pMMB503EH) and pCM93 (H505Y *fccA*/pMMB503EH). Expression in the Δ*fccA S. frigidimarina* strain EG301 (*3*) was carried out as described previously (*9*).

Protein Purification and Kinetic Analysis. Wild-type and mutant forms of Fcc_3 were purified as previously reported (*16*). Protein samples for crystallization and mass spectrometry were subjected to an additional purification step using FPLC with a 1-mL Resource Q column (Pharmacia) as described by Pealing et al. (*17*). Protein concentrations were determined using the Soret band absorption coefficient for the reduced enzyme (752.8 mM^{-1} cm^{-1} at 419 nm) (*16*).

The FAD content of Fcc_3 mutants was determined using the method of Macheroux (*18*), and all steady-state rate constants were corrected for the percentage of FAD present.

Mass spectrometry of proteins was carried out using a Micromass Platform II Electrospray mass spectrometer. Samples were prepared in 0.1% formic acid and introduced to the spectrometer via direct infusion. The spectrometer was standardized using horse heart myoglobin.

The steady-state kinetics of fumarate reduction were followed at 25.0 °C as described by Turner et al. (*19*). The fumarate-dependent reoxidation of reduced methyl viologen was monitored at 600 nm using a Shimadzu UV−PC 1501 spectrophotometer. To ensure anaerobicity, the spectrophotometer was housed in a Belle Technology glovebox under a nitrogen atmosphere with the O_2 level maintained well below 2 ppm. Assay buffers contained 0.45 M NaCl and 0.2 mM methyl viologen and were adjusted to the appropriate pH values using 0.05 M HCl or NaOH as follows: Tris/HCl (pH 7.0−9.0); MES/NaOH (pH 5.4−6.8); and CHES/NaOH (pH 8.6−10). The viologen was reduced by addition of sodium dithionite until a reading of around 1 absorbance unit was obtained (corresponding to around 80 μM reduced methyl viologen). The concentration of reduced methyl viologen could be varied between 100 and 20 μM with no effect on the rate of reaction. A known concentration of enzyme was added, and the reaction was initiated by addition of fumarate (0−1 mM).

Kinetic parameters K_m and k_{cat} were determined from the steady-state results using nonlinear regression analysis (Microcal Origin software). Profiles of pH versus maximum rate-constant were constructed by activity measurement under saturating substrate conditions at a range of pH values.

Crystallization and Refinement. Crystallization of H505A and H505Y flavocytochromes c_3 was carried out by hanging drop vapor diffusion at 4 °C in Linbro plates. Crystals were obtained with well solutions comprising 100 mM Tris-HCl buffer (pH 7.4−8.2) (measured at 25 °C), 80 mM NaCl, 16−19% PEG 8000, and 10 mM fumarate. Hanging drops of 4 μL were prepared by adding 2 μL of 6 mg/mL protein (in 10 mM TrisHCl, pH 8.5) to 2 μL of well solution. After approximately 10 days, needles of up to 1 × 0.2 × 0.2 mm and plates of up to 0.5 × 0.5 × 0.2 mm were formed. Crystals were immersed in a solution of 100 mM sodium acetate buffer, pH 6.5, 20% PEG 8000, 10 mM fumarate, and 80 mM NaCl, containing 23% glycerol as cryoprotectant, prior to mounting in nylon loops and flash-cooling in liquid nitrogen. For H505A flavocytochrome c_3, a data set was collected to 1.8 Å resolution at Daresbury synchrotron radiation source (Station 9.6, $\lambda = 0.979$ Å) using an ADSC Quantum 4 detector, and for H505Y flavocytochrome c_3, a data set was collected to 2.0 Å resolution at DESY in Hamburg (Station BW7B, $\lambda = 0.8459$ Å) using a Mar Research mar345 image plate detector. Crystals of both mutant forms were found to belong to space group $P2_1$. The H505A flavocytochrome c_3 crystal was found to have cell dimensions $a = 45.632$ Å, $b = 92.798$ Å, $c = 79.056$ Å, and $\beta = 91.02°$, while the H505Y flavocytochrome c_3 crystal was found to have cell dimensions $a = 76.989$ Å, $b = 87.274$ Å, $c = 89.366$ Å, and $\beta = 104.43°$.

Data processing was carried out using the HKL package (*20*). The wild-type Fcc_3 structure (1QJD), stripped of water, was used as the initial model for molecular replacement. Electron density fitting was carried out using the program Turbofrodo (*21*). Restraints for the FAD were calculated from two small molecule crystal structures (Cambridge Crystallographic Database codes HAMADPH and VEFHUJ10). Structure refinement was carried out using Refmac (*22*).

The atomic coordinates have been deposited in the Protein Data Bank [entries 1KSS (H505A) and 1KSU (H505Y)].

RESULTS

Characterization of Mutant Enzymes. The molecular masses of the mutant enzymes were determined by electrospray mass spectroscopy. In comparison to wild-type (63 033 Da, which includes the bound sodium ion), the mass difference was found to be −67 Da for H505A (expected difference of −66 Da) and +24 Da for H505Y (expected difference of +26 Da). These mass differences indicate that the sodium remains bound in both mutant enzymes. All the mutations were further verified by DNA sequencing. The average FAD content of the mutant enzymes was found to be 60%, H505A and 56%, H505Y. This is slightly lower than typical values for the recombinant wild-type enzyme of around 73%. All catalytic rates were corrected for the variation in FAD content.

Table 1: Comparison of k_{cat} and K_m Values for Wild-Type, H505A, and H505Y Forms of Fcc_3 (25 °C, $I = 0.45$ M)

	k_{cat} (s^{-1})			K_m (μM)		
pH	wild-type[a]	H505A	H505Y	wild-type[a]	H505A	H505Y
6.0	658 ± 34	32 ± 1	354 ± 19	43 ± 10	43 ± 6	22 ± 5
7.2	509 ± 15	79 ± 3	377 ± 29	25 ± 2	109 ± 13	25 ± 7
7.5	370 ± 10	101 ± 3	363 ± 29	28 ± 3	129 ± 10	17 ± 6
9.0	210 ± 13	105 ± 2	240 ± 5	7 ± 2	9 ± 1	21 ± 2

[a] Values for wild-type taken from ref 9.

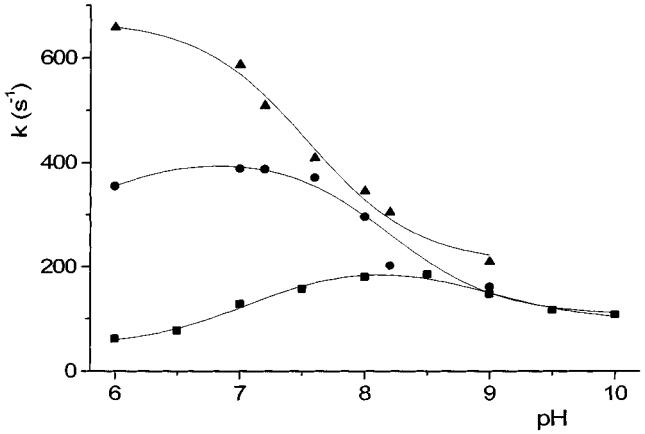

FIGURE 2: pH dependence of fumarate reductase activity (under saturating substrate conditions at 25 °C, $I = 0.45$ M: wild-type Fcc_3 (triangles); H505A Fcc_3 (squares); H505Y Fcc_3 (circles).

The ability of H505-substituted forms of Fcc_3 to catalyze fumarate reduction was determined over a range of pH values. The resulting k_{cat} and K_m parameters for wild-type and mutant forms of Fcc_3 are compared in Table 1. The pH profiles shown in Figure 2 show that the mutations have little effect on activity at high pH. However, as the pH is lowered, there is an increasing effect on activity. In fact, at pH 6.0 the k_{cat} value for the wild-type enzyme is some 20-fold higher than that for the H505A mutant. The wild-type enzyme exhibits a straightforward pH profile with a single pK_a of 7.5 ± 0.1 and with optimum activity below pH 6.0. In contrast, the two mutant enzymes show more bell-shaped pH profiles with two pK_a values of 7.1 ± 0.2 and 9.0 ± 0.2 determinable for H505A and one pK_a of 8.2 ± 0.1 for H505Y.

The Crystal Structures of the Mutant Flavocytochromes c_3. Data sets to a resolution of 1.8 Å (H505A) and 2.0 Å (H505Y) were used to refine the structures to final *R* factors of 15.64% (H505A, $R_{free} = 20.61\%$) and 16.70% (H505Y, $R_{free} = 23.86\%$) (Table 2). For the H505A mutant enzyme, the final model consists of one protein molecule comprised of residues 1−568, four hemes, the FAD, one substrate molecule (fumarate), and one sodium ion. In addition, the H505A model contains 1096 water molecules. In the case of the H505Y mutant enzyme, there are two molecules in the asymmetric unit so the final model consists of two protein molecules (with composition as described above) and a total of 1866 water molecules. For each protein molecule, three residues at the C-terminus (569−571) could not be located in the electron density maps. The rmsd fit of all backbone atoms for the wild-type and H505A mutant flavocytochromes c_3 is 0.3 Å, and for the wild-type and H505Y mutant enzyme the fit is also 0.3 Å, indicating no major differences between the structures. Because the H505Y crystal structure has two molecules in the asymmetric unit, the rmsd fit value stated is the average over both molecules (A and B).

Table 2: Data Collection and Refinement Statistics

	H505A	H505Y
resolution (Å)	20.0−1.8	20.0−2.0
total no. of reflections	318233	536347
no. of unique reflections	58239	77608
completeness (%)	95.4	99.2
$(I)/[\sigma(I)]$	18.5	11.3
R_{merge} (%)[a]	7.5	7.2
R_{merge} in outer shell (%)	18.5 (1.86−1.80 Å)	22.3 (2.07−2.00 Å)
R_{cryst} (%)[b]	15.64	16.70
R_{free} (%)[b]	20.61	23.86
rmsd from ideal values		
bond lengths (Å)	0.011	0.012
bond angles (deg)	2.2	2.4
Ramachandran analysis		
most favored (%)	87.9	89.0
additionally allowed (%)	12.1	10.8

[a] $R_{merge} = \sum_h \sum_i |I(h) - I_I(h)| / \sum_h \sum_i I_I(h)$, where $I_I(h)$ and $I(h)$ are the *i*th and mean measurement of reflection *h*, respectively. [b] $R_{cryst} = \sum_h |F_o - F_c| / \sum_h F_o$, where F_o and F_c are the observed and calculated structure factor amplitudes of reflection *h*, respectively. R_{free} is the test reflection data set, 5% selected randomly for cross validation during crystallographic refinement.

The crystal structures of the H505A and H505Y mutant enzymes do not show any unexpected structural changes compared to the wild-type structure (Figure 1). In the wild-type structure, His505 is seen to form a hydrogen bond with a water molecule (Wat912) at a distance of 2.9 Å, which in turn is part of the coordination sphere of the bound sodium ion, some 2.4 Å from the sodium. In the H505A mutant enzyme, the space vacated by the removal of the imidazole moiety is occupied by two water molecules, Wat2 and Wat147, which are 3.4 and 3.9 Å from the Ala505 side chain carbon, respectively (Figure 1). One of these water molecules, Wat2, is 3.1 Å from Wat48, which is in the equivalent position to that taken by Wat912 in the wild-type structure. Wat48 also ligates to the bound sodium ion at a distance of 2.5 Å. In the structure of the H505Y mutant Fcc_3, the tyrosine side-chain occupies the same position as that taken by the His505 side-chain in the wild-type structure (Figure 3). The hydroxyl group of the tyrosine is hydrogen-bonded to a water molecule (Wat41 in molecule A, Wat18 in molecule B) at 2.6 Å. These water molecules are shown to coordinate to the sodium ion at a distance of 2.5 Å. In all structures mentioned, the sodium ion is found in the same position.

The replacement of the histidine at position 505 has little structural effect at the active site even though it is adjacent to His504, a residue thought to be involved in both Michaelis complex formation and transition state stabilization. The bound fumarate assumes the same twisted conformation as observed for the hydroxylated, malate-like, molecule in the wild-type active site, and the important interactions required

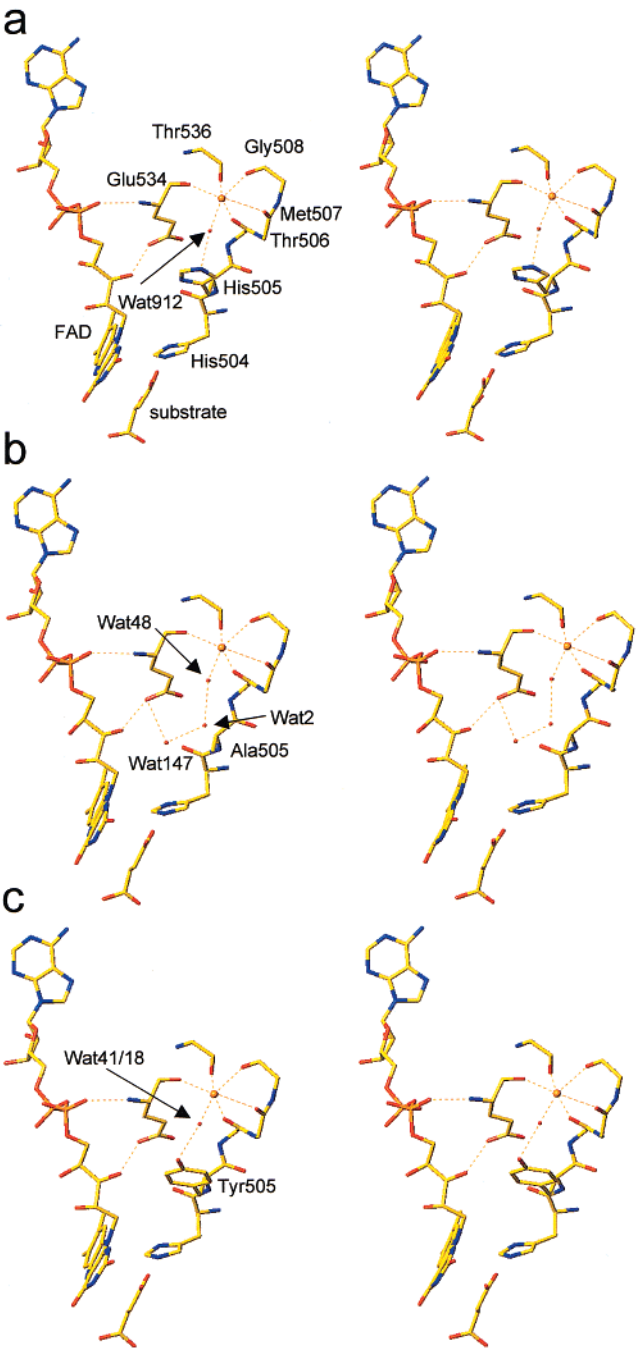

FIGURE 3: Stereoview of the region surrounding the sodium and the FAD in (a) wild-type, (b) H505A, and (c) H505Y flavocytochromes c_3. In each case, the sodium ion is shown as an orange sphere. The orange dotted lines indicate the coordination sphere of the sodium in each form of the enzyme, as well as some important hydrogen-bonding interactions. This diagram was generated using TURBO−FRODO (*21*).

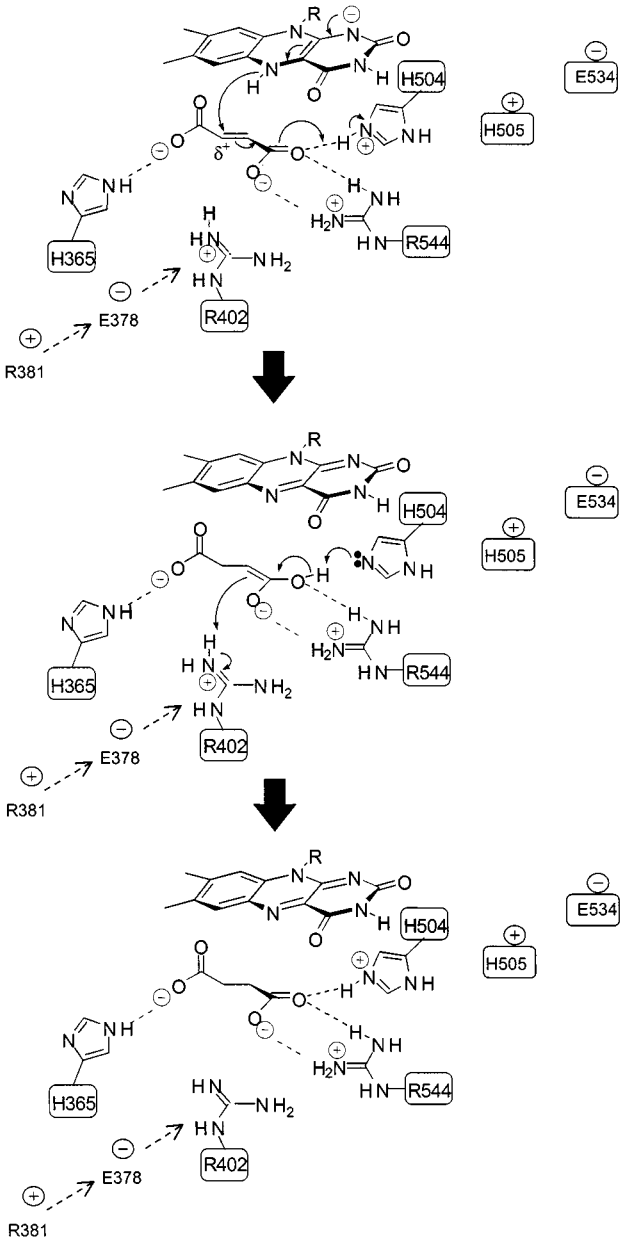

FIGURE 4: The reaction mechanism for fumarate reduction by Fcc_3 as originally proposed by Taylor et al. (*6*). Catalysis is initiated by the twisting out of plane of the C1 carboxylate group (on the left) of fumarate. The substrate is polarized by interactions with charged residues facilitating hydride transfer from N5 of reduced FAD to the substrate C2. The role of His504 is to stabilize the build up of negative charge on the substrate prior to protonation. Arg402 (3.0 Å from C3) is ideally positioned to donate a proton to substrate C3 resulting in the formation of succinate. Arg402 is immediately reprotonated via a proton pathway involving Arg381 and Glu378. The relative positions of His505 and Glu534 show schematically how His505 decreases the effect that the negative charge of Glu534 has on His504.

for catalysis (hydride transfer distance, proton delivery distance) are unaffected by the mutations.

DISCUSSION

The mechanism for the fumarate reductase (Fcc_3) catalyzed reaction, as originally proposed by Taylor et al. (*6*), is shown in Figure 4. In this mechanism His504 of Fcc_3 is shown protonating the C4 carboxylate to facilitate the transient formation of a carbanion at C3. Previous mutagenesis and pH studies indicated that a protonated His504 could enhance the rate of reaction but was not essential for it (*9*). This led to the suggestion that it was the imidazole of His504 that was responsible for the observed pK_a of around 7.5 seen in the wild-type enzyme. We have now shown that substitution of the adjacent residue, His505, can have significant effects on the pH dependence of Fcc_3. These are fairly modest for the H505Y mutation, with the largest effects on k_{cat} and K_m being less than 2-fold at pH 6.0, Table 1. However, in the case of the H505A mutation the effects are quite large with a 20-fold fall in the value of k_{cat} at pH 6.0.

It is clear that for both mutant enzymes there has been a shift in the pK_a value for enzyme activity. The most likely explanation is that substitution at position 505 has had an effect on the pK_a of the active site residue His504. Thus, the H505Y mutation appears to shift this pK_a from 7.5 to 8.2 and the H505A mutation from 7.5 to 9.0. The key question is, how do the substitutions at His505 modulate the pK_a of His504? The answer may lie in an examination of the three-dimensional structure of Fcc_3 in the region around His505. The imidazole ring of His505 lies between His504 and Glu534, and it is likely therefore that His505 helps to minimize the effect of the negative charge of Glu534 on His504. Removing the ring of His505, as is the case in the H505A mutant, would allow the charge on Glu534 to affect His504 making it a weaker acid. This is what seems to have happened since the pK_a shifts from 7.5 to 9.0 in the H505A mutant. The less pronounced effect seen for the H505Y mutation, on the other hand, is consistent with the phenol ring of the tyrosine being able to modulate the effect of the charge of Glu534 on His504. Indeed, it is not surprising that the H505Y mutation has a fairly modest effect, since the equivalent residue to His505 in most fumarate reductases (including the *E. coli* and *W. succinogenes* enzymes) is in fact a tyrosine.

In the wild-type Fcc_3 structure (*6*), His505 hydrogen bonds to a water molecule (Wat912) which is in the coordination sphere of the bound sodium ion. It is clear from the structures of the H505A and H505Y mutant enzymes that the replacement of the histidine does not significantly alter the inner-coordination sphere of the sodium ion (Figure 1). Two water molecules occupy the space vacated by the removal of the imidazole ring in the H505A. These form a hydrogen-bonding network to a water molecule which is in the equivalent position to that taken by Wat912 in the wild-type structure, and which ligates the sodium ion at a distance of 2.5 Å. In the H505Y structure, the tyrosine side-chain occupies approximately the same position as that taken by the imidazole ring of His505 in the wild-type structure (Figure 3). In this case, the hydroxyl group of the tyrosine hydrogen bonds to the water ligand. Thus, the sodium ion is found in essentially the same position in the wild-type and mutant structures of Fcc_3. An interesting question is how the sodium site in Fcc_3 compares to that seen in the other known fumarate reductase structures.

The structures of the fumarate reductases from *Shewanella oneidensis* MR1 (2.5 Å resolution) (*7*) and *E. coli* (3.3 Å resolution) (*1*) do not show any sodium ions assigned in the PDB files (1D4E and 1FUM, respectively). However, the arrangement of the protein backbone around the putative "sodium" site in these two enzymes is the same as in the wild-type Fcc_3 structure (1QJD, 1.8 Å resolution) (*6*). Clearly, the assignment of sodium would be difficult in these two lower resolution structures. Overall, however, the similarities between the structures of these enzymes would lead us to suggest that this sodium site is conserved throughout the fumarate reductase family.

In conclusion, we have demonstrated that His505 is not essential for sodium ion binding but may play a role in modulating the pK_a of a key active site residue, His504.

ACKNOWLEDGMENT

The authors would like to thank Dr. Marjorie Harding for helpful discussions.

REFERENCES

1. Iverson, T. M., Luna-Chavez, C., Cecchini, G., and Rees, D. C. (1999) *Science 284*, 1961−1966.
2. Körtner C., Lauterbach F., Tripier D., Unden G., and Kröger, A. (1990) *Mol. Microbiol. 4*, 855−860.
3. Gordon, E. H. J., Pealing, S. L., Chapman, S. K., Ward, F. B., and Reid, G. A. (1998) *Microbiology 4*, 937−945.
4. Lancaster, C. R. D., Kröger, A., Auer, M., and Michel, H. (1999) *Nature 402*, 377−385.
5. Lancaster, C. R. D., Groβ, R., and Simon, J. (2001) *Eur. J. Biochem. 268*, 1820−1827.
6. Taylor P., Pealing, S. L., Reid, G. A, Chapman, S. K., and Walkinshaw, M. D. (1999) *Nat. Struct. Biol. 6*, 1108−1112.
7. Leys, D., Tsapin, A. S., Nealson, K. H., Meyer, T. E., Cusanovich, M. A., and Van Beeumen, J. J. (1999) *Nat. Struct. Biol. 6*, 1113−1117.
8. Bamford, V., Dobbin, P. S., Richardson, D. J., and Hemmings. A. M. (1999) *Nat. Struct. Biol. 6*, 1104−1107.
9. Doherty, M. K., Pealing, S. L., Miles, C. S., Moysey, R., Taylor, P., Walkinshaw, M. D., Reid, G. A., and Chapman, S. K. (2000) *Biochemistry 39*, 10695−10701.
10. Reid, G. A., Miles, C. S., Moysey, R. K., Pankhurst, K. L., and Chapman, S. K. (2000) *Biochim. Biophys. Acta 1459*, 310−315.
11. Mowat, C. G., Moysey, R., Miles, C. S., Leys, D., Doherty, M. K., Taylor, P., Walkinshaw, M. D., Reid, G. A., and Chapman S. K. (2001) *Biochemistry 40*, 12292−12298.
12. Chapman, S. K., Morrison, C. A., Reid, G. A., Pealing, S. L., Taylor, P., and Walkinshaw M. D. (1999) in *Flavins and Flavoproteins 1999* (Ghisla, S., Kroneck, P., Macheroux, P., and Sund, H., Eds.) pp 105−113, Rudolf Weber, Agency for Scientific Publications, Berlin.
13. Kunkel, T. A., and Roberts, J. D. (1987) *Methods Enzymol. 154*, 367−382.
14. Sanger, F., Nicklen, S., and Coulson, A. R. (1977) *Proc. Natl. Acad. Sci. U.S.A. 74*, 5463−5467.
15. Michel, L. O., Sandkvist, M., and Bagdasarian, M. (1995) *Gene 152*, 41−45.
16. Pealing, S. L., Cheesman, M. R., Reid, G. A., Thomson, A. J., Ward, F. B., and Chapman, S. K. (1995) *Biochemistry 34*, 6153−6158.
17. Pealing, S. L., Lysek, D. A., Taylor, P., Alexeev, D., Reid, G. A., Chapman, S. K., and Walkinshaw, M. D. (1999*) J. Struct. Biol.* 127, 76−78.
18. Macheroux, P. (1999) in *Flavoprotein Protocols: Methods in Molecular Biology* (Chapman, S. K., and Reid, G. A., Eds.) Vol. 131, pp 1−7, Humana Press, Totowa, New Jersey.
19. Turner K. L., Doherty M. K., Heering H. A., Armstrong F. A., Reid G. A., and Chapman S. K. (1999) *Biochemistry 38*, 3302−3309.
20. Otwinowski, Z., and Minor, W. (1997) *Methods Enzymol. 276*, 307−326.
21. Roussel, A., and Cambillau, C. (1991) TURBO−FRODO, in *Silicon Graphics Geometry Partners Directory 86*, Silicon Graphics, Mountain View, CA.
22. Murshudov, G. N., Vagin, A. A., and Dodson, E. J. (1997) *Acta Crystallogr. D53*, 240−255.

BI020155E